Failure Avoidance in Wind Turbine Generator Systems

WP 1 : Deliverable 1.2

August 2, 2015

U. Shipurkar (TU Delft)

The objective of the project Design for Reliable Power Performance (D4REL) is: to improve the reliability and controllability of offshore wind turbines to reduce the operational uncertainty of future offshore wind power plants. Despite research in failures in electrical systems of wind turbines, they remain problematic and fail often. Work Package 1 of the project, in particular, deals with improving the availability of the electrical generator systems by using modular conversion system concepts that are fault tolerant, re-configurable and self-healing.

A powerful tool in designing for reliability is the use of fault avoidance. Since, this involves the elimination of certain failure mechanisms it can be very successful in improving the reliability of wind turbines. This report looks at some opportunities of using failure avoidance in wind turbine generator systems and represents the D4REL Deliverable 1.2 - 'Report on which failures could be avoided'.

This document discusses the opportunities for fault avoidance in the form of the following sections, Section 1 looks at using press-pack semiconductors to eliminate certain failure mechanisms in power semiconductors. Section 2 discusses the replacement of magnetic stator wedges with non-magnetic wedges. Section 3 introduces an improved brush-slip ring system that reduces wear, while Section 4 discuss the elimination of the brush-slip ring by the use of the Brushless Doubly Fed Induction Generator. Finally, Section 5 highlights opportunities in reliability oriented control.

1 Press-Pack Semiconductors

The power electronics have long been considered the 'bottleneck' in the reliability of wind turbine generator systems. Figure 1.1 shows the failure rates for components of the drivetrain and it shows that the power electronics suffer from high failure rates.

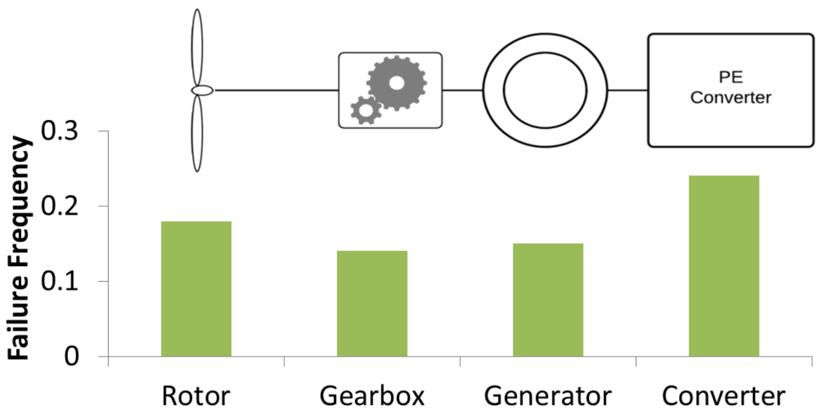

Figure 1.1: Overview of Drivetrain Sub-Assembly Failures [1]

Studies published by *Lyding et al.* and *Carroll et al.* give a component-wise failure distribution for the power electronic converter. These results are shown in Figure 1.2 and Figure 1.3 respectively. These studies show that the power semiconductor is a major contributor to the failure rates of the converter.

Deliverable 1.2 - Wind Turbine Generator Systems Failures - Probabilities and Mechanisms, has detailed the

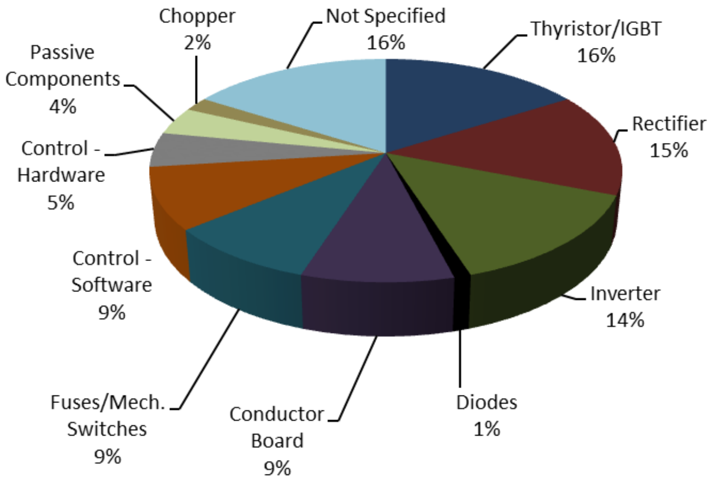

Figure 1.2: Share of Sub-Component Failure Rates in Power Electronic Assemblies [2]

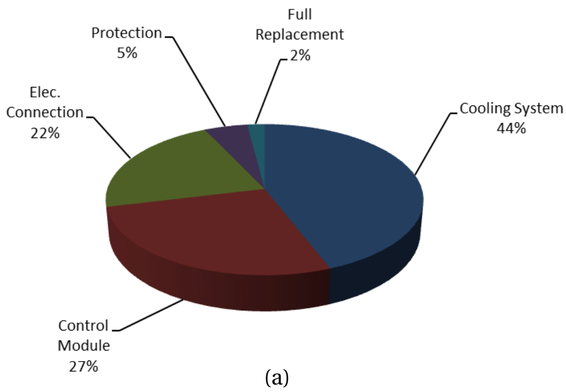

(a)

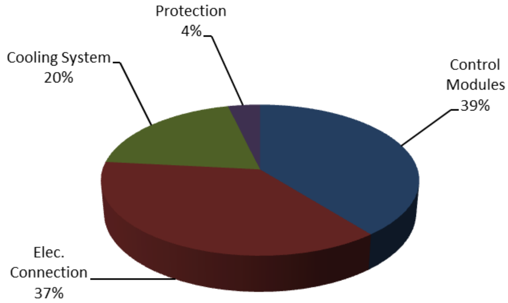

(b)

Figure 1.3: Share of Failures in Power Electronic Converters (a) for DFIG based drivetrains (b) for PMG based drivetrains [3]

failure mechanisms in power semiconductors. Solder joint fatigue is considered a major failure mechanism in power electronic components [4]. This failure occurs because the solder layer is subjected to mechanical stresses under temperature cycling, because of the difference in the Coefficient of Thermal Expansions (CTEs) of the two materials between which the solder is present.

IGBTs have two such joints - silicon chip and ceramic substrate, and ceramic substrate and base plate. Of these, the DCB ceramic-base plate solder joint is especially prone to failure due to a greater mismatch between the CTEs of the two materials resulting in shear stress in the solder layer and eventually cracks and voids [5]. Solder fatigue cracks are generally found close to the DCB ceramic due to higher temperatures. These cracks lead to a reduction in the heat conduction capability of the solder layer causing an increase in the temperature of the junction with further exacerbates the problem [6].

These effects may be a result of external heating (thermal cycling) or by internal heating due to losses in the

IGBT (power cycling) [7].

Another major failure is the lift-off of the bond wire. Bond wire lift-off has been considered as one of the principal forms of failures in IGBTs and diodes. Failure of wire bonds occur as a result of fatigue caused either by shear stresses generated between the chip and wire, or due to repeated flexure of the wire [6]. These develop as cracks propagating along the bond wire-chip interface due to thermo-mechanical stresses caused by temperature cycling and the fact that aluminium (bond wire material) and silicon (chip material) have very different Coefficient of Thermal Expansion (CTE) [8]. However the use of improved bonding methods, protection layers [7] and molybdenum-aluminium strain buffers [6] have reduced these failures to such an extent that they do not seem to pose any particular threat to IGBT reliability.

Considering these major failure mechanisms, new packaging technologies have been developed to improve performance and replace wirebonds. These are solder interconnects and pressure contacts [9]. Table 1.1 gives an overview of failure mechanisms of these three packaging technologies.

Table 1.1: Overview of Failures in Power Semiconductors [9] [6] [5]

	Chip and Wire	**Direct Solder Interconnect**	**Press-Pack Technology**
Wire Lift-off	X		
Wirebond Fatigue	X		
Solder Fatigue	X	X	
DBC Cracking	X	X	
Die Attach Fatigue	X	X	X
Si Device Cracking	X	X	X
Spring Fatigue			X
Spring Stress Relaxation			X
Surface Wear			X

The press-pack technology uses pressure to obtain electrical and thermal contacts, thus eliminating wire-bonds and minimising solder connections. The structure of press-pack IGBTs has been discussed widely in literature [9, 10, 11, 12, 13],Figure 1.4 shows this overall structure. Even though the wirebonds and solder based failure modes are eliminated, the press-pack suffers from other failure modes. One is the reduction in contact force may increase the contact resistance raising the junction temperature and exposure to corrosion. Also, the spring experiences thermal fatigue due to thermal cycling [9].

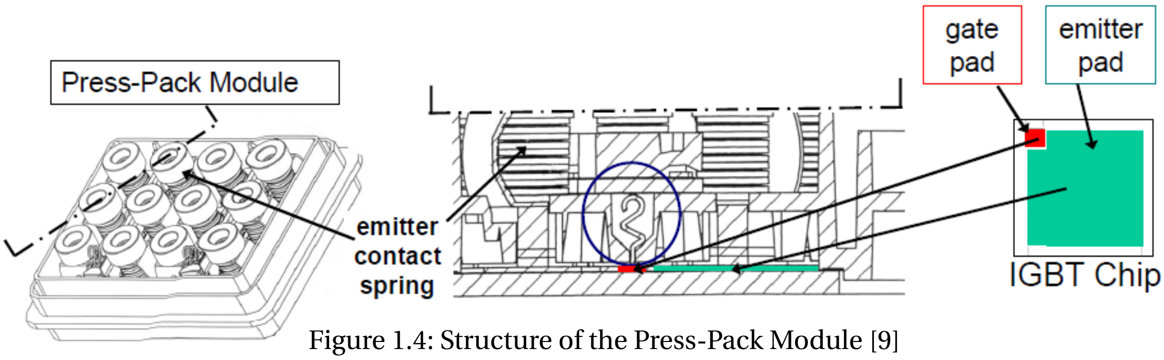

Figure 1.4: Structure of the Press-Pack Module [9]

Despite these 'new' failure modes, reliability is the major advantage offered by the press-pack IGBT. *Benavides et al.* compared the reliability of the press-pack and flat-pack IGBTs (The major failure mode for the flat-pack IGBT is the thermal failure of the solder [14]). This comparison was done for thermal cycling failure modes, which is the major failure mode. Figure 1.5 shows the results of this study. This comparison shows

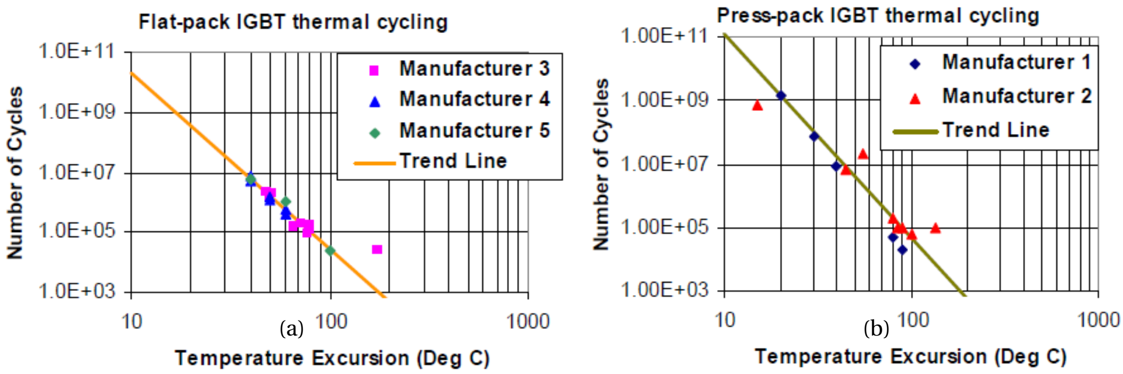

Figure 1.5: Comparison of Thermal Cycling Lifetime for (a) Flat-Pack IGBT and, (b) Press-Pack IGBTs [15]

that the press-pack technology increases reliability by 350% which is a large improvement.

Tinschert et al. also investigated the failure modes in press-pack IGBTs [16]. Their tests found the devices failing earlier than expected. They hypothesised that the failures occurred due to damage of the gate-oxide and micro-eroding which is supported by FEM simulations. However, further investigation is required.

2 Magnetic Wedges

Alewine et al. studied the failures of wind turbine generators and found that approximately 15% of failures in generators rated above 2MW were due to stator wedges [17]. One explanation of this is that when magnetic stator wedges are used, they are subjected to pulsating forces which speed up the failure process.

Magnetic wedges offer a number of improvements to machines resulting in increased efficiency [18, 19, 20]. However, looking at their propensity to failure in wind turbines, it may be important to look at their impact once again. Here, the generator designs developed by *Polinder et al.* in [21] are used to analyse and compare the effective improvements in different types of generator technologies.

As in [21] this paper uses a 3MW turbine for the study, the final paper will contain details. This paper looks at the effect of magnetic stator wedges for wind turbines with four different generator technologies. These are,

- Doubly Fed Induction Generator (DFIG) with a three stage gearbox, or DFIG3G.
- Permanent Magnet Direct Drive Generators (PMDD) without a gearbox.
- A Permanent Magnet Generator with a single stage gearbox, or PMG1G.
- A DFIG with a single stage gearbox, or DFIG1G.

2.1 Modelling Magnetic Wedges

The modelling of the turbine rotor, gearbox, converter and generator has already been detailed in [21]. This section only looks at the aspects that are effected by the inclusion of magnetic wedges. Figure 2.1 shows the structure of a stator slot with a smooth rotor and marks the parameters used in the rest of this section.

The modelling detailed in this section is based on [22], where other sources have been used, they will be mentioned in the text.

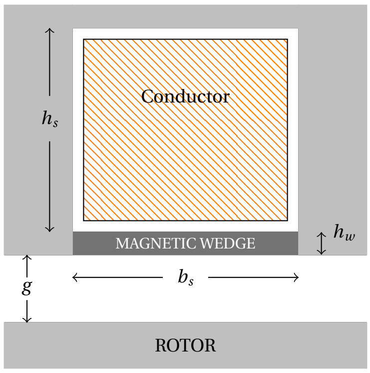

Figure 2.1: Structure of Slot

EFFECT ON AIRGAP - The main effect of the magnetic wedge is that is reduces the effective airgap. The slots in a machine cause a decrease in flux density at the slot opening.

This is modelled by calculating an effective airgap based on the Carter principle. The slots result in an increased effective airgap. When magnetic wedges are used, this increase in the effective airgap length due to the Carter factor is reduced. This is shown in Equation 2.1.

$$\begin{aligned}
\kappa &= \frac{2}{\pi}\left[\arctan\left(\frac{b_s}{2g\mu_{wedge}}\right) - \frac{2g}{b_s} ln\sqrt{1+\left(\frac{b_s}{2g\mu_{wedge}}\right)^2}\right] \\
k_C &= \frac{\tau_u}{\tau_u - \kappa b_s} \\
g_{eff} &= k_C g
\end{aligned} \tag{2.1}$$

The magnetic wedge reduces the effective slot width, thereby reducing the Carter factor and therefore the effective airgap. For a permanent magnet machine, the equation for the effective airgap is modified as in Equation 2.2.

$$g_{eff} = k_C\left(g + \frac{l_m}{\mu_{rm}}\right) \tag{2.2}$$

EFFECT ON MAGNETIZING INDUCTANCE - As in [21] the magnetizing inductance depends on the effective airgap and is given by Equation 2.3.

$$L_{sm} = \frac{6\mu_0 l_s r_s (k_w N_s)^2}{p^2 g_{eff} \pi} \tag{2.3}$$

where, l_s is stack length, r_s is stator radius, k_w is winding factor and N_s is number of turns of the phase winding. The reduction in the effective airgap due to the magnetic wedge will result in an increase in the magnetizing inductance.

EFFECT ON LEAKAGE INDUCTANCE - There are three components of the leakage inductance considered; the slot leakage, the tooth tip leakage and the end winding leakage. The end winding leakage remains unaffected by the inclusion of magnetic wedges and therefore is not discussed here.

The slot leakage inductance is caused by the leakage of flux over the slots of the machine. This can be calculated using the magnetic energy stored in the slot and the value of this inductance is expressed in Equation 2.4.

$$L_{\sigma,s} = \frac{2\mu_0 l_s N_s^2}{pq} \left(\frac{h_s}{3b_s} + \frac{\mu_{wedge} h_w}{b_s} \right) \tag{2.4}$$

The tooth tip inductance is caused by the leakage flux in the air-gap outside the slot opening. The inductance is calculated by applying a permeance factor and is shown in Equation 2.5.

$$L_{\sigma,t} = \frac{2\mu_0 l_s N_s^2}{pq} \left[\frac{5\frac{\mu_{wedge} g}{b_s}}{5 + 4\frac{\mu_{wedge} g}{b_s}} \right] \tag{2.5}$$

2.2 Magnetic Wedges in DFIGs

For the performance of the DFIGs all harmonics have been neglected. In reality, the inclusion of stator magnetic wedges will reduce slot harmonics and hence iron losses. Another aspect that has not been considered in this study is the thermal model of the machine. The inclusion of the magnetic wedges with its ferrite content may improve the thermal conduction of the machine.

For the two DFIG machine designs, detailed in Table 2.1, the optimal μ_{wedge} for maximum energy extraction is calculated. These are shown in Figure 2.2 and Figure 2.3.

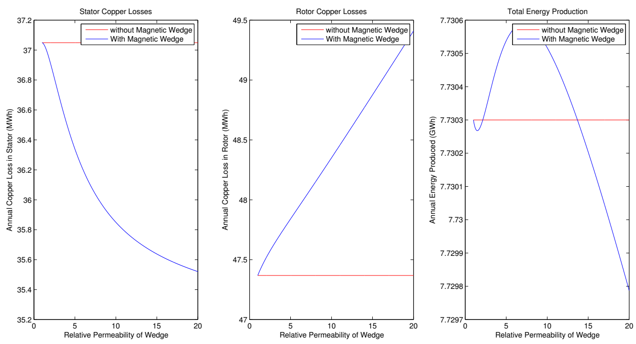

Figure 2.2: Variation of Annual Power Quantities with μ_{wedge} for DFIG with 3 stage Gearbox

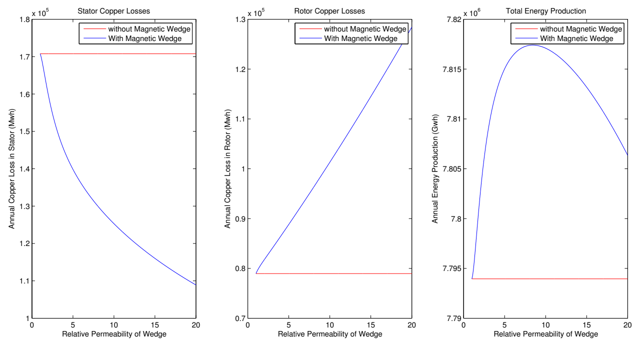

Figure 2.3: Variation of Annual Power Quantities with μ_{wedge} for DFIG with 1 stage Gearbox

2.3 Magnetic Wedges in PM Generators

For the performance of the Permanent Magnet Generators as well, all harmonics have been neglected. In reality, the inclusion of stator magnetic wedges will reduce slot harmonics and hence iron losses. Also, the eddy current losses in the rotor magnets have been neglected.

For the two PM machine designs, detailed in Table 2.1, the optimal μ_{wedge} for maximum energy extraction is calculated. These are shown in Figure 2.4 and Figure 2.5.

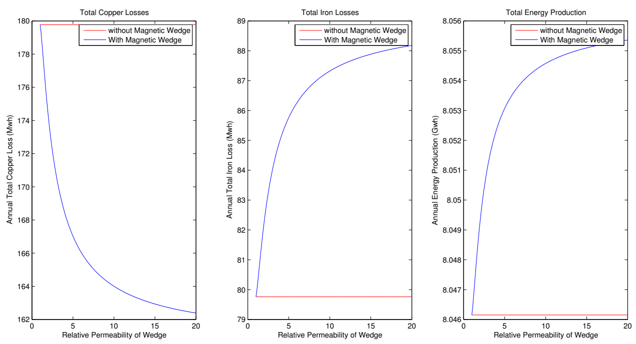

Figure 2.4: Variation of Annual Power Quantities with μ_{wedge} for Direct Drive PM Generator

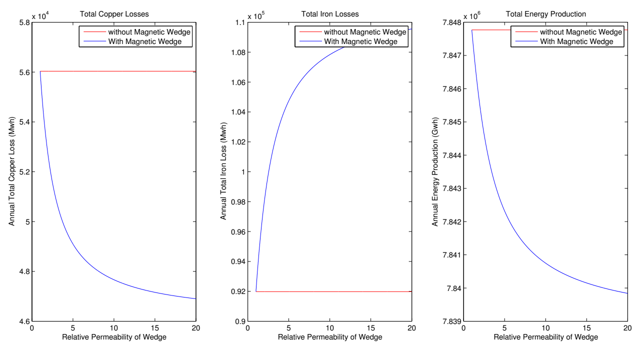

Figure 2.5: Variation of Annual Power Quantities with μ_{wedge} for PM Generator with 1 stage Gearbox

2.4 Improvement with Magnetic Wedges

The improvement in efficiency and the increased energy yield is shown in Table 2.1. Further, the efficiency curves are given in Figure 2.6.

	DFIG		**PM Synchronous**	
	3 stage Gearbox	**1 stage Gearbox**	**Direct Drive**	**1 stage Gearbox**
Generator Dimensions				
Stator Radius (m)	0.42	2.0	2.5	1.88
Stack Length (m)	0.75	0.5	1.2	0.37
Number of Pole Pairs	3	35	80	35
No. of Slots per Pole per Phase	6	6	1	1
Air-gap (mm)	1	4	5	3.8
Stator Slot Width (mm)	12.9	8.5	15	24.8
Stator Tooth Width (mm)	11.5	6.4	18	31.4
Stator Slot Height (mm)	60	80	80	80
Stator Yoke Height	100	50	40	40
Rotor Slot Width (mm)	10	7.9	-	-
Rotor Tooth Width (mm)	11.5	6.4	-	-
Rotor Slot Height (mm)	60	80	-	-
Rotor Yoke Height (mm)	100	50	40	40
Magnet Height (mm)	-	-	15	15
Rotor Pole Width (mm)	-	-	79	168
WITHOUT Magnetic Wedges				
Annual Energy Values				
Copper Losses (MWh)	84.41	249.72	179.77	56.03
Iron Losses (MWh)	69.74	123.60	79.76	91.98
Converter Losses (MWh)	77.72	66.49	229.27	228.22
Gearbox Losses (MWh)	532.94	266.46	-	272.45
Total Losses (MWh)	764.81	706.27	488.8	648.40
Energy Yield (GWh)	7.73	7.79	8.04	7.85
WITH Magnetic Wedges				
Optimum μ_{wedge}	9.09	9.3	10	-
Annual Energy Values				
Copper Losses (MWh)	83.44	211.08	164.00	56.03
Iron Losses (MWh)	69.74	123.60	87.32	91.98
Converter Losses (MWh)	77.72	66.49	229.05	228.22
Gearbox Losses (MWh)	532.94	266.46	-	272.45
Total Losses (MWh)	763.84	667.63	480.37	648.40
Energy Yield (GWh)	7.73	7.83	8.05	7.85
Difference in Energy Yield (MWh)	**0.97**	**38.64**	**8.42**	**0**

Equivalent hrs. of Production	**1.1**	**43.43**	**9.16**	**0**

Table 2.1: Comparison of Effect of Magnetic Wedges on Different Generator Systems

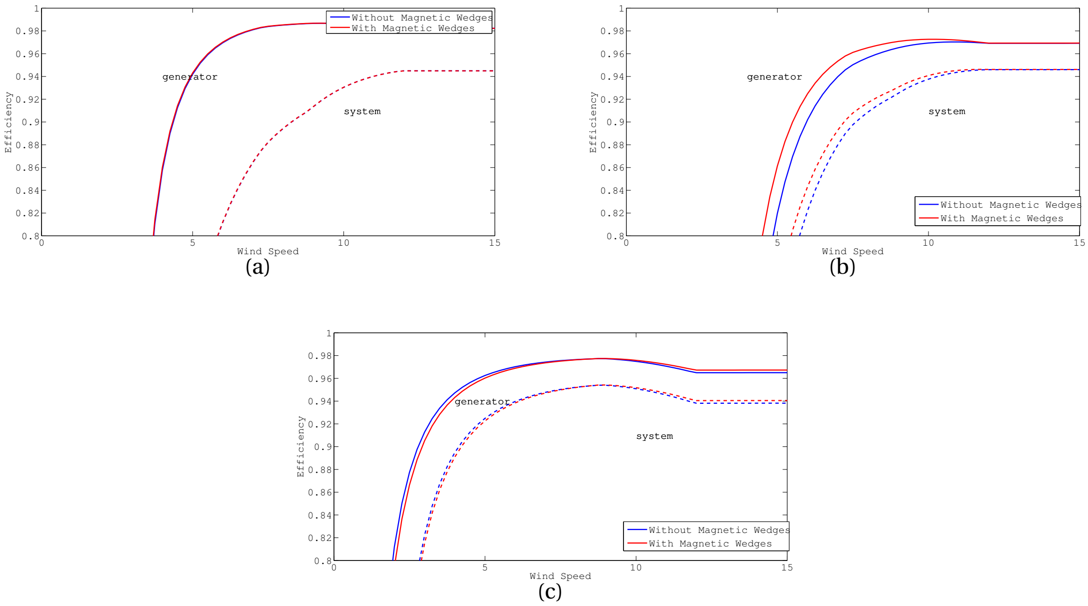

Figure 2.6: Efficiency for (a) DFIG3G, (b) DFIG1G and, (c)PMDD based Wind Turbines

2.5 Conclusions and Future Work

These results show that the advantage offered by the inclusion of magnetic wedges is small. Therefore, replacing the magnetic wedges with non-magnetic wedges could increase reliability without a large effect on energy production, leading to a net reduction in Cost of Energy (CoE). However, a number of factors need to be looked into further,

- This study has been conducted only on theoretical generator models. It would be important to test the improvement, due to magnetic wedges, with practical and real machine designs. This could result in greater increase in energy production with magnetic wedges.
- The improvement has been based on using a wedge with an optimal magnetic permeability. In reality the magnetic wedges may not have these properties. Therefore, the improvement shown here may be optimistic.
- For a better insight into the use of magnetic wedges, the cost of maintenance due to failures in the wedges should be compared with the cost of the extra energy produced.

3 Improved Brush-Slip Ring System

A majority of wind turbines employ the DFIG in the drivetrain. *Carroll et al.* studied the failures in DFIGs from a certain manufacturer. Figure 3.1 shows the results of their findings.

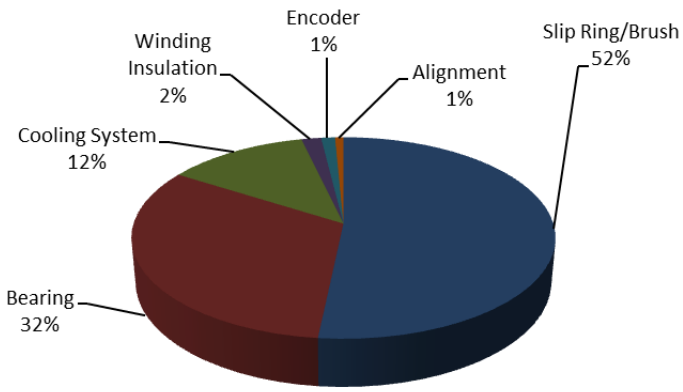

Figure 3.1: Share of Sub-Component Failure Rates in DFIGs [3]

It can be seen that more than half the failures are brush-slip ring failures. Even though more than half these failures are classified as minor failures (Figure 3.2), for far offshore wind turbines minor failures can be very expensive as well.

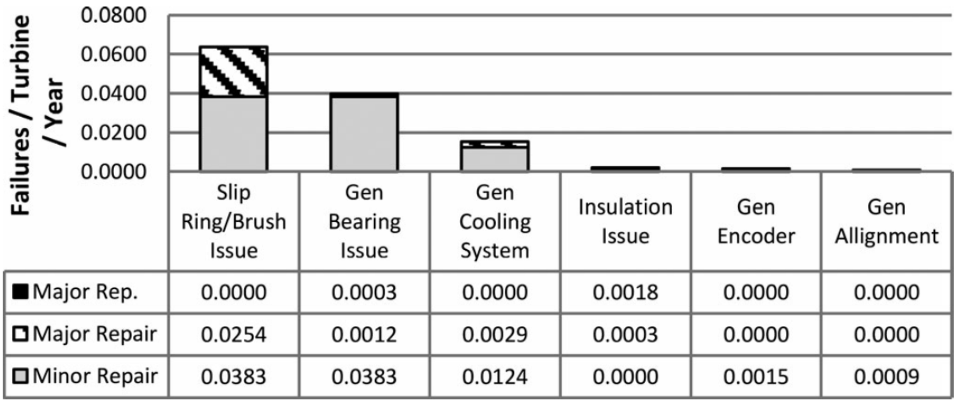

Figure 3.2: Severity of Failures in DFIG [3]

Therefore, addressing the failures in the brush-slip ring system can help increase the reliability of the DFIG based wind turbines. One of the ways of doing this is to use lubricated contacts thus reducing wear and hence failure rates. Such a system also aims at reducing the contact resistance which could help in the thermal management of the generator.

3.1 Theory of Lubricated Contacts

The friction coefficient and hence the wear of lubricated contacts is governed by the Stribeck Curve [23, 24]. This curve is shown in Figure 3.3. The operation of the contacts occurs in three regimes. The *boundary lubrication* regime there is metal-metal contact. However, the coefficient of friction is still considerable less than in the 'dry' state. Since there is metal-metal contact, the contact resistance should be the lowest in this regime. In the *hydrodynamic lubrication* regime the two surfaces are completely separated by a lubricating film. As expected, the friction coefficient is the lowest in this regime, although this rises as the film thickness rises. As there is a film of lubricant separating the contacts, the contact resistance in this regime is large. The *mixed lubrication* regime lies in between the other two regimes.

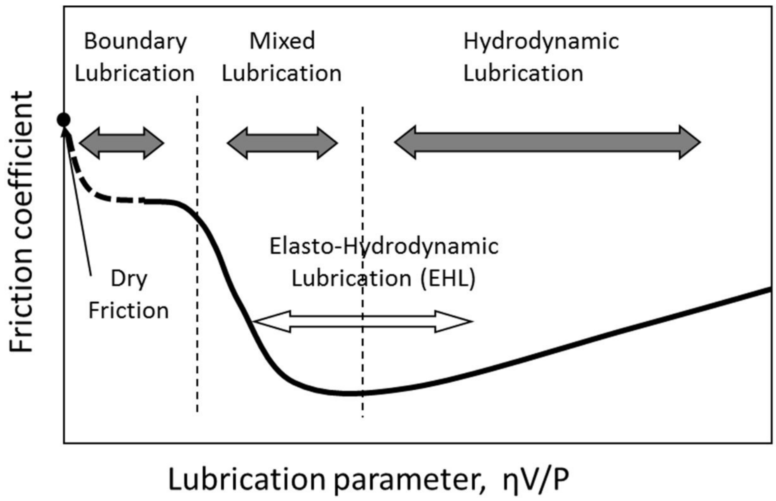

Figure 3.3: Stribeck Curve [24]

3.2 Experimental Setup

To study the improvements offered by lubricated contacts for use in DFIG based systems a experimental setup as shown in Figure 3.4 was built.

The aim is to compare the performance of the lubricated and the 'dry' brush systems in terms of voltage drop across the contacts and the wear in the brushes. The oil used is a colloidal graphite oil patented by Rotelcon BV.

3.3 Initial Experimental Results

3.3.1 Test on Oil

The first set of test are to determine the properties of the oil used. It is hypothesised that the colloidal graphite contained in the oil forms parallel paths when the lubricating oil thickness is small and hence reduce the

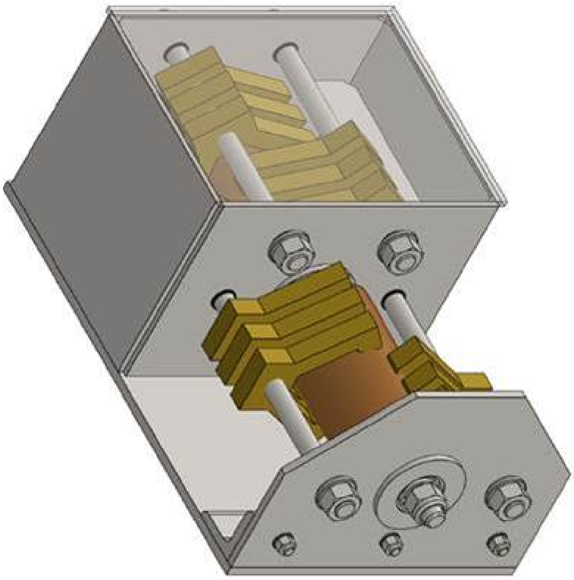

Figure 3.4: Experimental Setup

contact resistance. Hence, this lubricating oil should offer low contact resistance until a certain oil thickness when the colloidal graphite chains are broken.

To test this a setup as shown in Figure 3.5 is employed.

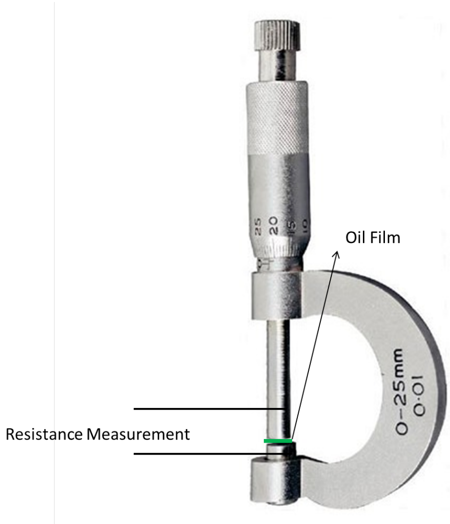

Figure 3.5: Oil Experiment Setup

This setup is used to test the hypothesis stated above. The reading of the screw-gauge is the thickness of the oil film and the resistance is measured across the two arms of the gauge. Therefore, the value of resistance measured is only an indicative value that can be used for comparison.

Figure 3.6 shows the contact resistance for two stationary contacts with the oil.

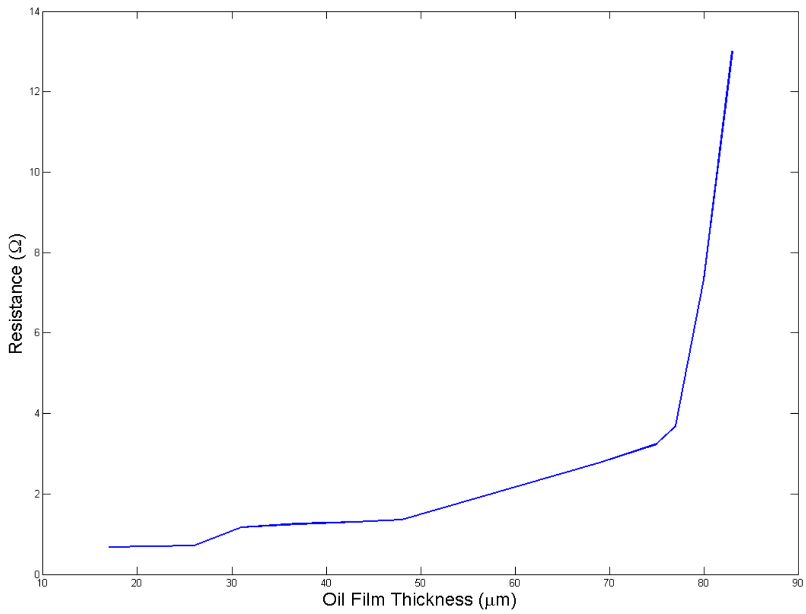

Figure 3.6: Resistance between Terminals vs. Oil Film Thickness

A further test is performed with no oil and two control oil samples (olive oil and sunflower oil). The results are shown in Figure 3.7.

A number of observations are made on the basis of these tests,

- The resistance plot in Figure 3.6 shows a knee point at approximately $80\mu m$. This indicates the expected film thickness to transition from boundary lubrication to hydrodynamic lubrication.
- The no oil curve in Figure 3.7 shows that the surface roughness no longer plays a role after the contacts are separated by approximately $20\mu m$. The fact that the 'brush' oil has a knee point at a much larger film thickness supports the hypothesis that the colloidal graphite improves contact resistance.
- The control oils, test oil 1 and 2, show that the improved results are a property of the 'brush' oil.

The results support the hypothesis, but further testing is required before the hypothesis can be confirmed.

3.3.2 Testing on Brush-Slip Ring Setup

Initial testing was done with bulk oil that was applied to the shaft by running the shaft through the oil. The results on a stationary shaft shows that there is improvement with the 'wet' brushes, i.e. the brush set using the 'brush' oil. Figure 3.8 shows the voltage drop across the two sets of brushes.

However, as the speed of the shaft increases the force of the oil pressure to cause the 'wet' brushes to lift-

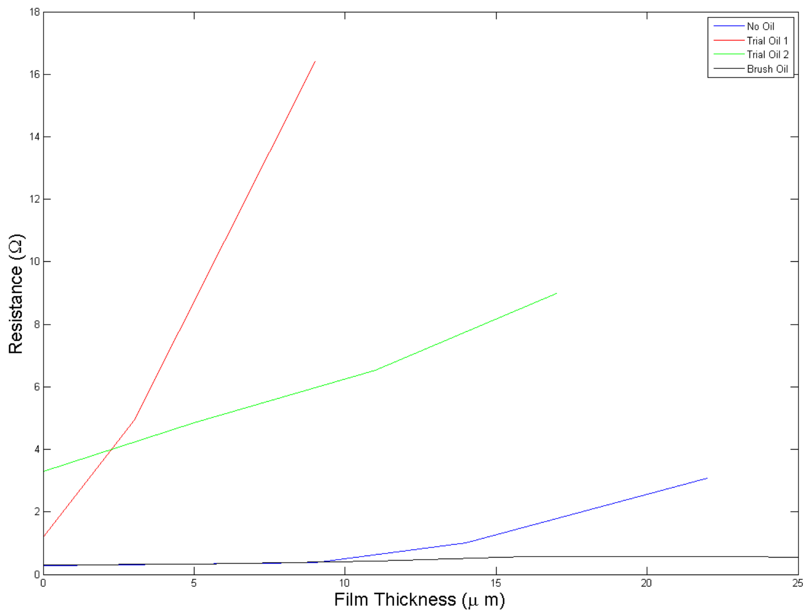

Figure 3.7: Resistance Comparison for Different Oils

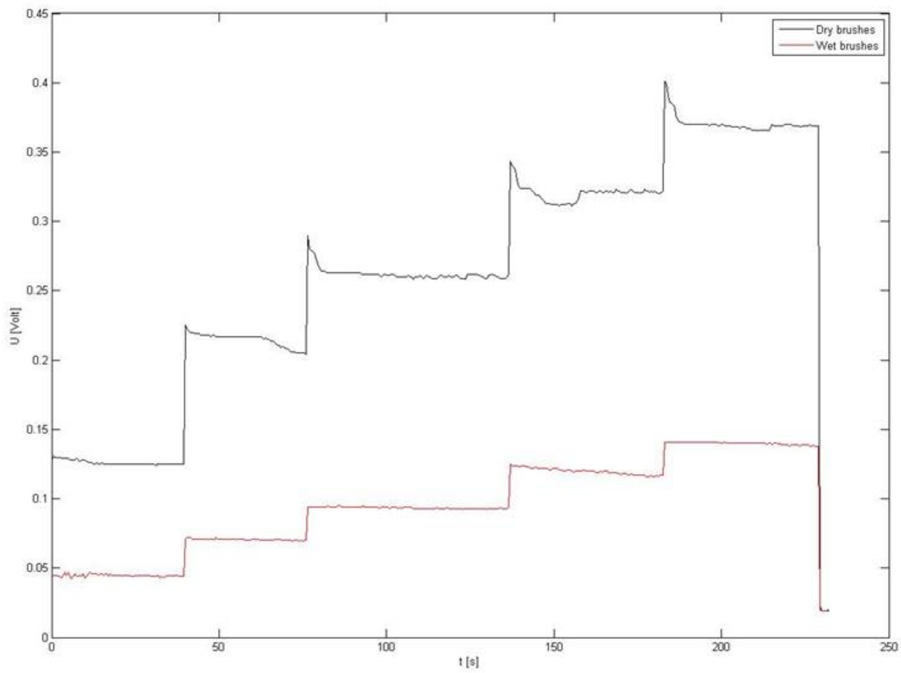

Figure 3.8: Resistance Comparison for 'Wet' and 'Dry' Brushes at Standstill

off, thus increasing the voltage drop. Figure 3.9 shows the voltage drop at 500rpm and 1000rpm. The brush lift-off can be seen in the results at 1000rpm.

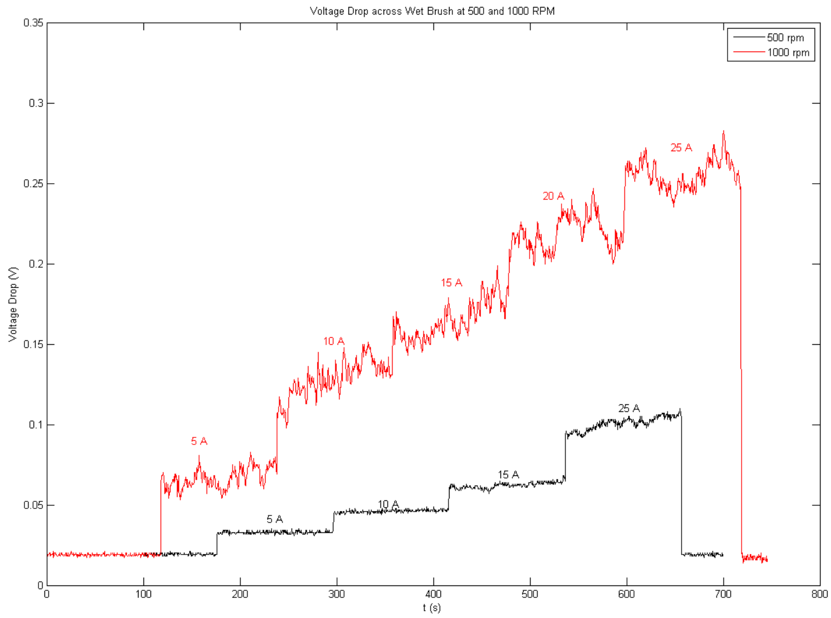

Figure 3.9: Comparison of Voltage Drop of the 'Wet' Brushes at 500rpm and 1000rpm

To improve performance, especially at higher speeds, another method of oil application was used. Strips of felt that apply the oil on the shaft by drawing the oil out of the reservoir using capillary action were used and an improvement in the speed range was found. However, further testing is required.

3.4 Conclusions and Future Work

Initial tests show that using brush-slip rings lubricated with the 'brush' oil could improve the performance and improve the wear of brushed systems. These could not only improve the reliability of DFIGs but also be applied to the brushes used in the blade pitch system.

However, further research is required. Some of the other aspects to be researched further are,

- Mapping the contact resistance/voltage drop on the Stribeck curve.
- Comparison of performance with DC, AC and, PWM based supplies. This includes the voltage drop and wear rates.
- Effect on wear with the lubricated brushes, especially considering the effect of DC current flow direction.
- Comparing the results using different brush types, such as carbon brushes which are widely used in wind turbines.

4 Brushless Doubly Fed Induction Generator

Section 3 has described the failure rates of Brush-Slip Rings systems. As the failures account for approximately half of all DFIG failures, improving the reliability of the brush-slip ring system can have a major effect on the reliability of a wind turbine. Avoiding failure by eliminating the need for brushes is a powerful way of doing this.

Therefore, the Brushless Doubly Fed Induction Machine (B-DFM or B-DFIG) is an attractive solution. Section 4.1 and Section 4.2 on machine description and operation have been taken from reference - [25].

4.1 Machine Description

The B-DFIM has two sets of 3-phase windings with different pole numbers. One of these windings is termed the 'Power Winding' while the other 'Control Winding'. For machine operation the Power Winding is connected directly to the supply while the Control Winding is connected through a partially rated power electronic converter. Figure 4.1 shows a schematic representation of a wind turbine drivetrain with the B-DFIM.

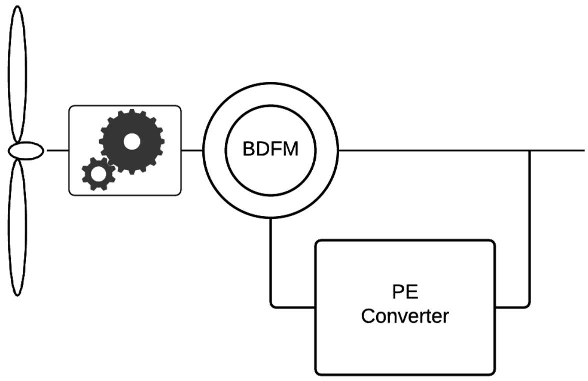

Figure 4.1: Schematic of B-DFIM based Wind Turbine Drivetrain

4.2 Machine Operation

The nested-loop rotor couples the power and control winding. The synchronous mode of operation occurs due to the coupling of the two stator windings (with different pole numbers) through the rotor [26]. In this arrangement, the Power Winding is connected to the supply while the Control Winding is supplied with a voltage of variable frequency as shown in Figure 4.1.

When the power winding is connected to the grid, the voltage and frequency are constant. The control winding frequency is determined by the shaft speed through (4.1) [26]. The control winding voltage is used to control the reactive power absorbed/generated by the machine.

$$\omega_m = \frac{\omega_p + \omega_c}{p_p + p_c} \tag{4.1}$$

4.3 Conclusions and Future Work

The B-DFIG is yet to be commercialised for use in wind turbine generators. *McMahon et al.* have designed and tested a 250kW prototype [27]. However, there are no manufacturers that offer B-DFIG based wind turbines yet.

Further,

- The B-DFIG eliminates the need of brushes/slip rings. This can be especially beneficial for wind turbines in offshore applications.
- Due to the structure of the B-DFIG design, it has higher values of leakage inductance. This results in lower efficiencies. However, the trade-off between higher reliability and lower efficiencies needs to be explored further.
- One advantage of the B-DFIG is its improved low voltage ride through capability [28]. The B-DFIG is able to handle low voltage events without the use of an extra crowbar circuit. Therefore, the power electronic converter is protected without the use of extra components, improving reliability.
- TU Delft has been successful in demonstrating sensor-less control of the B-DFIG. By eliminating the encoder, the sensor-less method further boosts reliability.

5 Reliability Oriented Control

Conventional control schemes for wind turbines are based on the extraction of maximum energy from the wind. However, considering the cost of maintenance for far offshore wind turbines, it may be important to look at reliability oriented control strategies.

This section makes the case for the development of reliability oriented control strategies based on a comparison of the simulated lifetime consumption in power electronic switches under different wind speed regimes. In particular it describes the tool that has been developed and could be used to investigate such a proposition.

5.1 Background

Reliability of wind turbines is a critical factor from the point of view of reducing the Cost of Energy (CoE). The drivetrain of the wind turbine remains a major contributor to the total failures occurring [1]. The power electronics, in particular, has become a 'bottleneck' with respect to reliability.

The research on reliability is moving from statistics based approach to a physics based approach [29, 30]. One of the tools for this is stress and strength modelling [29]. Stress modelling maps the stresses encountered by the wind turbine while strength modelling uses the knowledge of the physics-of-failure to draw correlations between the applied stresses and fatigue. Such a tool can be invaluable in giving realistic estimates for the lifetime of wind turbine components and computing the effectiveness of the design and other reliability based control strategies.

Aalborg University has considerable experience with such stress and strain modelling. In collaboration with them a tool has been created that calculates the consumed lifetime of power semiconductors for a given wind profile. This tool is used to compare the lifetime consumption for three different wind regimes. These wind regimes are based on mean speeds of 8, 10, and 12 m/s. Offshore sites generally have high average wind speeds, as an example the KNMI data collection station F3-FB-1 sees a mean wind speed of 10m/s [31]. Therefore, offshore wind turbines could benefit from reliability based controls. The next few sections describe the tool developed and the results of simulations conducted for different wind regimes.

5.2 Reliability Tool

The structure of the tool is shown in Figure 5.1.

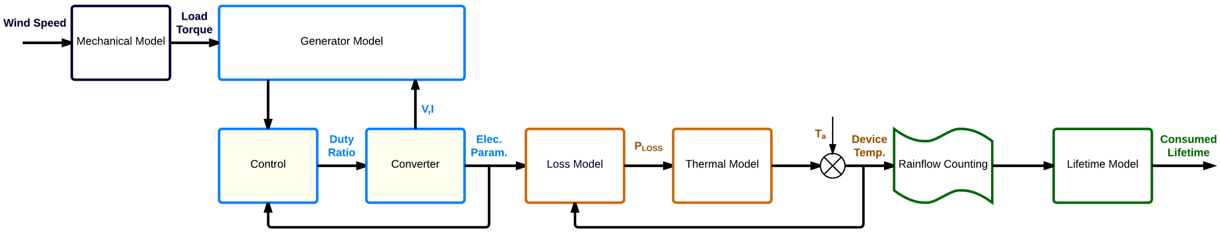

Figure 5.1: Schematic for Lifetime Estimation Tool

The input to the model is the wind speed. This is fed to the mechanical model which generates the load torque signal for the generator. The generator is controlled for maximum power extraction. Based on the generator, control block and converter models, the required electrical parameters are generated. These are used by the power semiconductor loss model to calculate the losses in the switches and diodes. This is converted to a temperature signal by the thermal model of the power semiconductors. Further, a rainflow counter and lifetime models are used to calculate the consumed lifetimes.

Table 5.1 gives the characteristics of the wind turbine used in the modelling.

Table 5.1: Wind Turbine Characteristics

	DFIG	**PMDD**
Rated Grid Power	2 MW	2 MW
Rotor Diameter	71 m	71 m
Optimal Tip Speed Ratio	8	8
Max. Power Coefficient	0.48	0.48

The modelling of the DFIG and PMSG has been extensively covered in literature [32, 33, 34, 35]. The models used in this study have been developed for 2MW machines with parameters given in Table 5.2.

Table 5.2: 2MW Generator Parameters [36]

	DFIG	PMDD
Rated Power	2 MW	2 MW
Pole Pairs	2	102
Gear Ratio	95	-
Rated Shaft Speed	1800 rpm	19 rpm
Stator Leakage Inductance	0.038 mH	0.276 mH
Magnetising Inductance	2.91 mH	
Rotor Leakage Inductance	0.064 mH	-
Stator/Rotor Turns Ratio	0.369	-

For the back to back converters, multiple parallel converters are modelled. For the PMSM, 4 parallel converters are used while for the DFIG, 2 parallel converters are modelled. Further, a power device rated at 1700V/1000A is used. Details of the modelled converters is given in Table 5.3.

Table 5.3: Back to Back Converter Data [36]

	DFIG	PMDD
Parallel Converters	2	4
Rated Active Power	400 kW	500 kW
DC-Link Voltage	1150 V	
Switching Frequency	2 kHz	
Grid Side Converter		
Rated Output Voltage	704 V	704 V
Filter Inductance	0.5 mH	0.15 mH
Generator Side Converter		
Rate Output Voltage	560 V	760 V

The control of a wind turbine is based on three control loops,

- Pitch control - The pitching of the blades is undertaken to regulate the power output or the speed of the turbine. This control is active above rated wind speeds and at start-up or shut-down of the turbine.
- Torque Control - This control loop is applied on the wind turbine generator to regulate the power and speed below rated speeds. This control loop is based on maximum power extraction from the wind resource.
- Yaw Control - This is used to 'point' the turbine in the wind direction. However, this is not modelled in this work.

In the tool developed only pitch and generator torque control have been modelled. These are well established in literature [34, 37, 38]. The control algorithm for generator torque control implemented in this paper is based on the vector control of the generators for maximum power extraction.

5.3 Simulation Results

The aim is to investigate the lifetime consumption of the power semiconductors under different wind regimes. The wind regimes were generated for one hour long periods using the *Wind Turbine Blockset* [39] with different mean wind speeds, of 8 m/s, 10 m/s, and 12 m/s. Figure 5.2 shows the wind speed with time for the three regimes considered.

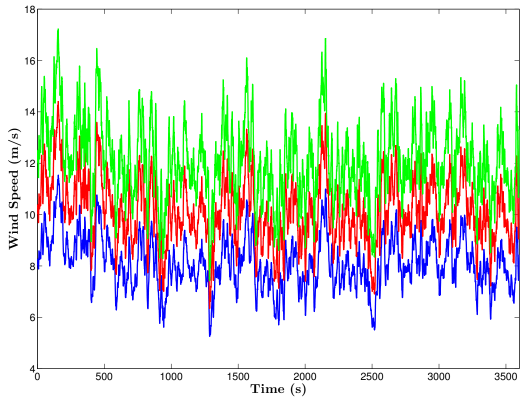

Figure 5.2: Wind Speed Regimes

The results of the thermal model for a PM Direct Drive based drivetrain is shown in figures 5.3a - 5.4c. Similarly, the results of the thermal model for a DFIG based drivetrain is shown in figures 5.5a - 5.6c. These figures show the junction temperature of the grid side and generator side converters for the three different wind regimes.

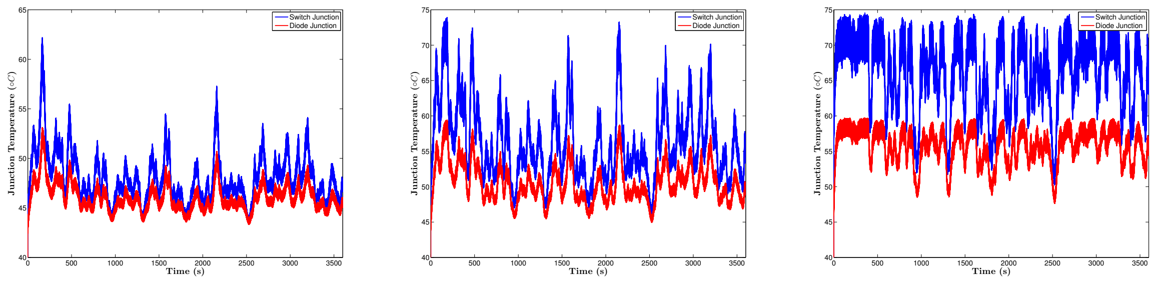

(a) Mean Wind Speed of 8m/s (b) Mean Wind Speed of 10m/s (c) Mean Wind Speed of 12m/s

Figure 5.3: Junction Temperature Results for PMDD based Drivetrain Grid Side Converter for different Wind Regimes

Based on these temperature distributions, the consumed lifetime has been calculated based on models developed at Aalborg University. The results of this consumed lifetime calculation is given in Table 5.4.

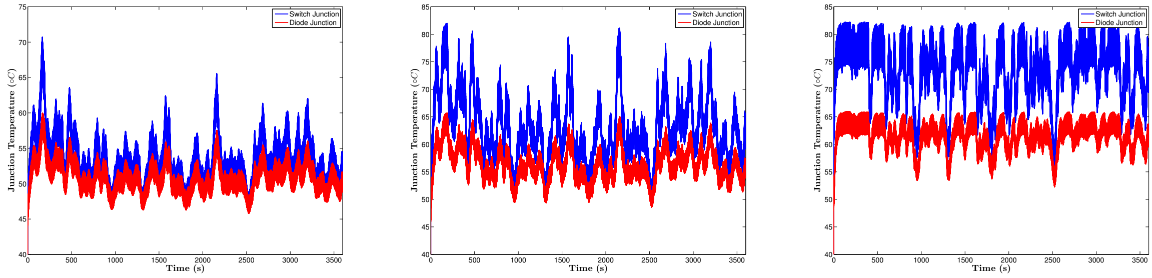

(a) Mean Wind Speed of 8m/s (b) Mean Wind Speed of 10m/s (c) Mean Wind Speed of 12m/s

Figure 5.4: Junction Temperature Results for PMDD based Drivetrain Generator Side Converter for different Wind Regimes

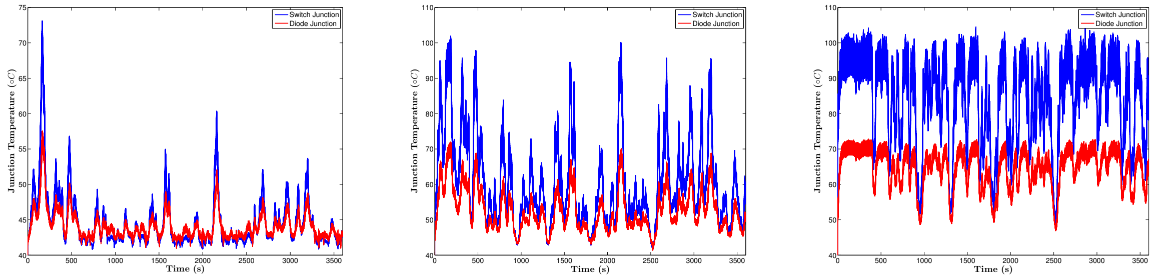

(a) Mean Wind Speed of 8m/s (b) Mean Wind Speed of 10m/s (c) Mean Wind Speed of 12m/s

Figure 5.5: Junction Temperature Results for DFIG based Drivetrain Grid Side Converter for different Wind Regimes

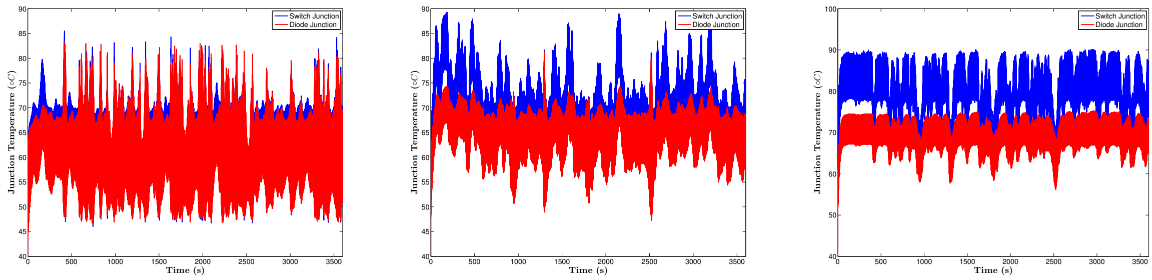

(a) Mean Wind Speed of 8m/s (b) Mean Wind Speed of 10m/s (c) Mean Wind Speed of 12m/s

Figure 5.6: Junction Temperature Results for DFIG based Drivetrain Generator Side Converter for different Wind Regimes

5.4 Conclusions

It is evident that operating at higher wind speeds lead to a higher consumption of lifetime in the power semiconductor devices. It therefore stands to reason that the benefits of a shift towards a reliability oriented control could offset the reduction in power generation and lead to a reduced cost of energy.

Table 5.4: Lifetime Consumption for 1hr in Different Wind Regimes

Chip Solder Fatigue		
Mean Wind Speed (m/s)	**PMDD based Drivetrain**	**DFIG based Drivetrain**
8	5.51E-07	3.71E-06
10	7.85E-06	2.42E-04
12	8.76E-06	3.77E-04

However, further research is required and the simulations shown here only set the stage for this by developing the tools required for such a study. In particular, the following aspects should be investigated further,

- the possibility of using circulating currents within the paralleled converters to reduce temperature swings and reduce lifetime consumption,
- the possibility of using de-rating based on consumed lifetime to prolong life in converters.

References

[1] F. Spinato, P. Tavner, G. van Bussel, and E. Koutoulakos, "Reliability of wind turbine subassemblies," *IET Renewable Power Generation*, vol. 3, no. 4, p. 387, 2009. [Online]. Available: http://digital-library.theiet.org/content/journals/10.1049/iet-rpg.2008.0060

[2] P. Lyding, S. Faulstich, B. Hahn, and P. Tavner, "Reliability of the Electrical Parts of Wind Energy Systems - a Statistical Evaluation of Practical Experiences," in *EPE Wind Energy Chapter Symposium*, 2010.

[3] J. Carroll, A. McDonald, and D. McMillan, "Reliability Comparison of Wind Turbines with DFIG and PMG Drive Trains," *IEEE Transactions on Energy Conversion*, vol. 30, no. 2, pp. 663–670, 2015.

[4] K. Fischer, T. Stalin, H. Ramberg, T. Thiringer, J. Wenske, and R. Karlsson, "Investigation of Converter Failure in Wind Turbine," Elforsk, Tech. Rep., 2012.

[5] C. Busca, R. Teodorescu, F. Blaabjerg, S. Munk-Nielsen, L. Helle, T. Abeyasekera, and P. Rodriguez, "An overview of the reliability prediction related aspects of high power IGBTs in wind power applications," *Microelectronics Reliability*, vol. 51, no. 9-11, pp. 1903–1907, Sep. 2011. [Online]. Available: http://linkinghub.elsevier.com/retrieve/pii/S0026271411002526

[6] M. Ciappa, "Selected failure mechanisms of modern power modules," *Microelectronics Reliability*, vol. 42, no. 4-5, pp. 653–667, Apr. 2002. [Online]. Available: http://linkinghub.elsevier.com/retrieve/pii/S0026271402000422

[7] H. Berg and E. Wolfgang, "Advanced IGBT modules for railway traction applications: Reliability testing," *Microelectronics Reliability*, vol. 38, no. 6-8, pp. 1319–1323, Jun. 1998. [Online]. Available: http://linkinghub.elsevier.com/retrieve/pii/S0026271498001504

[8] S. Ramminger, P. Türkes, and G. Wachutka, “Crack mechanism in wire bonding joints,” *Microelectronics Reliability*, vol. 38, no. 6-8, pp. 1301–1305, Jun. 1998. [Online]. Available: http://linkinghub.elsevier.com/retrieve/pii/S0026271498001413

[9] P. Hansen and P. McCluskey, “Failure models in power device interconnects,” in *2007 European Conference on Power Electronics and Applications, EPE*, 2007.

[10] F. Wakeman, G. Lockwood, and M. Davies, “New high reliability bondless pressure contact IGBTs,” in *PCIM Europe Conference Proceedings*, 1999, pp. 67–72.

[11] F. Wakeman, K. Billett, R. Irons, and M. Evans, “Electromechanical characteristics of a bondless pressure contact IGBT,” *APEC ’99. Fourteenth Annual Applied Power Electronics Conference and Exposition. 1999 Conference Proceedings (Cat. No.99CH36285)*, vol. 1, no. 44, pp. 312–317, 1999.

[12] S. Eicher, M. Rahimo, E. Tsyplakov, D. Schneider, A. Kopta, U. Schlapbach, and E. Carroll, “4.5kV press pack IGBT designed for ruggedness and reliability,” *Conference Record - IAS Annual Meeting (IEEE Industry Applications Society)*, vol. 3, pp. 1534–1539, 2004.

[13] S. Kaufmann, T. Lang, and R. Chokhawala, “Innovative press pack modules for high power IGBTs,” *Proceedings of the 13th International Symposium on Power Semiconductor Devices & ICs. IPSD ’01 (IEEE Cat. No.01CH37216)*, no. June, pp. 1–4, 2001.

[14] H. Kirihata, Y. Takahashi, H. Wakimoto, and F. Niino, “Investigation of flat-pack IGBT reliability,” *Conference Record of 1998 IEEE Industry Applications Conference. Thirty-Third IAS Annual Meeting (Cat. No.98CH36242)*, vol. 2, pp. 1016–1021, 1998.

[15] N. Benavides, T. McCoy, and M. Chrin, “Reliability Improvements in Integrated Power Systems with Pressure-Contact Semiconductors,” in *Proc. ASNE*, 2009.

[16] L. Tinschert, A. R. Å rdal, T. Poller, M. Bohlländer, M. Hernes, and J. Lutz, “Possible failure modes in Press-Pack IGBTs,” *Microelectronics Reliability*, vol. 55, no. 6, pp. 903–911, 2015. [Online]. Available: http://linkinghub.elsevier.com/retrieve/pii/S0026271415000451

[17] K. Alewine and W. Chen, “A review of electrical winding failures in wind turbine generators,” in *2011 Electrical Insulation Conference (EIC)*. IEEE, Jun. 2011, pp. 392–397. [Online]. Available: http://ieeexplore.ieee.org/lpdocs/epic03/wrapper.htm?arnumber=5996185

[18] K. Alewine and C. Wilson, “Magnetic wedge failures in wind turbine generators,” *2013 IEEE Electrical Insulation Conference, EIC 2013*, no. June, pp. 244–247, 2013.

[19] M. Davis, “Problems and Solutions with Magnetic Stator Wedges,” in *IRIS Rotating Machine Conference*, 2007. [Online]. Available: http://msdn.microsoft.com/en-us/magazine/ff798279.aspx

[20] R. Curiac and H. Li, “Improvements in energy efficiency of induction motors by the use of magnetic wedges,” in *2011 Record of Conference Papers Industry Applications Society 58th Annual IEEE Petroleum and Chemical Industry Conference (PCIC)*. IEEE, Sep. 2011, pp. 1–6. [Online]. Available: http://ieeexplore.ieee.org/lpdocs/epic03/wrapper.htm?arnumber=6085890

[21] H. Polinder, F. F. a. Van Der Pijl, G. J. De Vilder, and P. J. Tavner, "Comparison of direct-drive and geared generator concepts for wind turbines," *IEEE Transactions on Energy Conversion*, vol. 21, no. 3, pp. 725–733, 2006.

[22] J. Pyrhönen, T. Jokinen, and V. Hrabovcová, *Design of Rotating Electrical Machines*. Wiley, 2008.

[23] J. Lemaitre, Ed., *Handbook of Materials Behavior Models*. Elsevier Inc., 2001.

[24] Y. Kondo, T. Koyama, and S. Sasaki, "Tribological Properties of Ionic Liquids," 2013. [Online]. Available: http://www.intechopen.com/books/ionic-liquids-new-aspects-for-the-future/tribological-properties-of-ionic-liquids

[25] U. Shipurkar, "Brushless Double Fed Induction Generator Based Wind Turbine Drivetrain under Grid Fault Conditions," M.Sc. Thesis, Delft University of Technology, 2014.

[26] S. Williamson, A. C. Ferreira, and A. K. Wallace, "Generalised theory of the brushless doubly-fed machine . Part I : Analysis," *IEE Proceedings - Electric Power Applications*, vol. 144, no. 2, pp. 111–122, 1997.

[27] R. McMahon, E. Abdi, P. D. Malliband, S. Shao, M. E. Mathekga, and P. J. Tavner, "Design and testing of a 250 kW medium-speed Brushless DFIG," *International Conference on Power Electronics, Machines and Drives*, pp. 0–5, 2012. [Online]. Available: http://ieeexplore.ieee.org/xpls/abs_all.jsp?arnumber=6242172

[28] U. Shipurkar, T. D. Strous, H. Polinder, and J. A. Ferreira, "LVRT Performance of Brushless Doubly Fed Induction Machines - A Comparison," in *presesnted at IEMDC*, 2015.

[29] F. Blaabjerg, "Future on Power Electronics for Wind Turbine Systems," *IEEE Journal of Emerging and Selected Topics in Power Electronics*, vol. 1, no. 3, pp. 139–152, 2013. [Online]. Available: http://ieeexplore.ieee.org/lpdocs/epic03/wrapper.htm?arnumber=6573352

[30] H. Wang, M. Liserre, and F. Blaabjerg, "Toward reliable power electronics: Challenges, design tools, and opportunities," *IEEE Industrial Electronics Magazine*, vol. 7, no. 2, pp. 17–26, 2013.

[31] "KNMI Data Centre - Observations, model forecasts and projections." [Online]. Available: https://data.knmi.nl/portal/KNMI-DataCentre.html#

[32] R. Pena, J. Clare, and G. Asher, "Doubly fed induction generator using back-to-back PWM converters and its application to variable-speed wind-energy generation," p. 231, 1996.

[33] J. Slootweg, H. Polinder, and W. Kling, "Dynamic modelling of a wind turbine with doubly fed induction generator," *2001 Power Engineering Society Summer Meeting. Conference Proceedings (Cat. No.01CH37262)*, vol. 1, pp. 644–649, 2001.

[34] Y. Errami, M. Maaroufi, and M. Ouassaid, "Modelling and control strategy of PMSG based variable speed wind energy conversion system," *Multimedia Computing and Systems (ICMCS), 2011 International Conference on*, no. 2, pp. 1–6, 2011.

[35] P. Kundur, *Power Systems Stability and Control*, 1st ed. McGraw-Hill Education, 1994.

[36] D. Zhou, F. Blaabjerg, M. Lau, and M. Tonnes, "Thermal analysis of multi-MW two-level wind power converter," in *IECON Proceedings (Industrial Electronics Conference)*, 2012, pp. 5858–5864.

[37] O. Anaya-Lara, N. Jenkins, J. Ekanayake, P. Cartwright, and M. Huges, *Wind Energy Generation: Modelling and Control*. Wiley, 2009.

[38] A. Tapia, G. Tapia, J. Ostolaza, and J. Saenz, "Modeling and control of a wind turbine driven doubly fed induction generator," *IEEE Transactions on Energy Conversion*, vol. 18, no. 2, pp. 194–204, Jun. 2003. [Online]. Available: http://ieeexplore.ieee.org/lpdocs/epic03/wrapper.htm?arnumber=1201089

[39] F. Iov, A. D. Hansen, P. Sorensen, and F. Blaabjerg, "Wind Turbine Blockset in Matlab/Simulink," Aalborg University, Tech. Rep., 2004.